Opportunities for Soft Electrohydraulic Actuation for Burrowing in Dry and Submerged Granular Media

Hoseung Seo[1], Eric Acome[2], Nicholas Kellaris[2], Shane Mitchell[2], Nathan Rohrbaugh[2], Yeonwook Roh[1], Nick Gravish[1], and Michael T. Tolley[1]

***Abstract*— Development of robotic platforms capable of burrowing in granular media (GM) has shown potential for applications in agriculture, construction of infrastructure, and extraterrestrial exploration. A promising strategy for burrowing is the use of high-frequency vibration to locally fluidize the GM to reduce drag forces. However, there have been few implementations of this method for robotic burrowers. In this work, we explore the use of hydraulically amplified, self-healing electrostatic (HASEL) actuators for soft robots capable of burrowing in dry and submerged GM. We propose that HASEL actuators can achieve both high-frequency vibration to fluidize GM and low-frequency, high-strain actuation for effective burrowing. We present a prototype multi-segmented robot design using HASEL actuators. We evaluate the drag reduction effects of high-frequency HASEL actuation in GM, and investigate the locomotion properties of the multi-segmented robots on the surface of, and burrowing inside, GM. We also demonstrate the capability of our actuators to detect obstacles within GM, and analyze the power consumption and operational endurance of our system. This work opens up opportunities for the future use of HASEL actuators for soft burrowing robots.**

I. Introduction

Development of robotic platforms capable of burrowing in granular media (GM) such as sand is crucial for applications including agriculture, construction of infrastructure, and extraterrestrial exploration. However, despite numerous recent advancements, robotic burrowing in GM presents significant challenges, as the surrounding grains can generate large drag forces as well as exhibit both solid-like and liquid-like characteristics [1]. To address these issues, numerous works have taken inspiration from biological burrowers to develop novel locomotion strategies in GM [2].

One of the ways organisms facilitate burrowing is by fluidizing the GM to effectively reduce drag forces in the direction of burrowing. Several bivalve mollusk species [3] and Pacific Sandfish [4], found in wet granular environments, extract water from the surroundings and eject it into the GM, temporarily suspending the granular particles in the fluid and allowing the body to advance quickly before the particles settle and reconsolidate [5]. Octopuses also jet water into the seabed, using fluidization as the primary method to burrow themselves [6]. Inspired by these organisms, previous works have explored flow-based local fluidization for burrowing, such as a vine-inspired robot that jets air into dry GM to reduce drag [7] and a robot that uses a jet of water to burrow into submerged GM [8]. However, these methods require large pumps or fluid reservoirs to maintain constant flow of fluid [2], which limits their potential for development of untethered robotic systems.

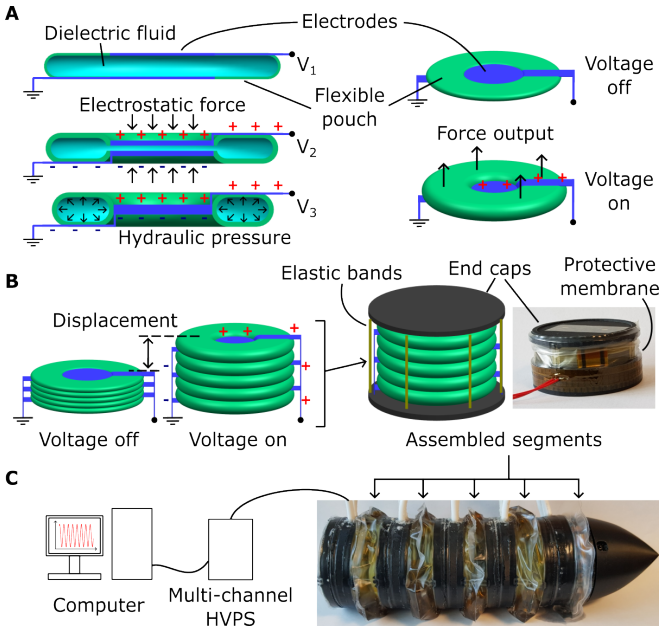

Fig. 1. Design of the HASEL-based burrowing robotic system. A) We used expanding circular HASEL actuators for our system [15], [18]. When we applied an electrical potential to a set of electrodes, opposing charges on the electrodes caused the electrodes to attract, displacing the dielectric fluid in between ($V_1 < V_2 < V_3$ in the diagram). The displaced fluid then induced hydraulic pressure within the flexible pouch, causing the actuators to expand and output force in the direction normal to the electrode surface. B) We stacked multiple HASELs to increase the total displacement. Each actuator segment was assembled from 20 HASEL actuators, polymer end caps, elastic bands to provide restoring force, and encapsulating flexible membrane to protect and electrically insulate the actuators. C) We assembled the multi-segmented robots with five to seven actuator segments and a rigid conical tip. Each segment could be individually controlled using a multi-channel high-voltage power supply (HVPS).

An alternative approach is to use high-frequency vibration to induce fluidization of the surrounding GM, which results in reduced drag forces [9]. This effect has been studied for bulk fluidization of tank filled with GM [10], [11], surface locomotion on GM [12], and reducing penetration resistance of an intruder [13]. However, there has been limited work in implementation for robotic burrowers, save for a robotic anchor that combined vibration-based fluidization and variable density induced by volume change to burrow and unburrow

*This work was supported by the Office of Naval Research, grant numbers N00014-22-1-2595, N00014-23-1-2169 and N00014-23-1-2358.

[1]Department of Mechanical and Aerospace Engineering, University of California, San Diego (UCSD), La Jolla, CA, USA, 92093 tolley@ucsd.edu

[2]Artimus Robotics, 2985 Sterling Ct Suite B, Boulder, CO, USA, 80301 eric@artimusrobotics.com

out of GM [14]. In this example, vibration was achieved with a DC motor, and a pneumatic bladder was used to tune effective density. As a result, locomotion was limited to the vertical direction only. Achieving locomotion in any other direction (e.g. horizontal) requires a different mechanism for moving through the GM.

Hydraulically amplified, self-healing electrostatic (HASEL) actuators are a relatively new type of soft actuator with muscle-like performance [15]–[17]. HASELs use electrostatic forces to generate local hydraulic pressure in flexible structures filled with liquid dielectrics [15]. Since the fluid motion in HASELs is limited as compared to other fluidic actuation mechanisms, they incur minimal viscous losses, allowing them to function over a wide range of actuation frequencies while still being able to achieve large strain [18]. Furthermore, HASEL actuators are lightweight, compact, and capable of self-sensing their configuration [15], [19], [20]. Due to their versatility, they have been used for various soft robotic applications, including bio-mimetic muscles [21], appendages [22]–[24], swimming robots [25], [26], and peristaltic robots capable of surface locomotion [27], [28].

In this work, we explore the use of HASEL actuators for soft robots capable of horizontal digging in dry and submerged GM. We propose that the unique combination of capabilities of HASEL actuators is promising for the development of compact burrowing robots: 1) HASELs can vibrate at high frequencies [18], which shows potential for local fluidization of GM for reduced drag forces; 2) the high strain of HASEL actuators [15], [18] indicates their capacity for the stroke required for horizontal burrowing; 3) the self-sensing capability of HASELs [15], [19], [20] could enable the robots to detect obstacles within GM that are not readily visible from the outside. The sections that follow present the evaluation of these critical capabilities. In Section II, we describe a prototype design of HASEL-based actuator segments and multi-segmented robots. In Section III, we perform drag tests in GM to explore the drag reduction effects of high-frequency HASEL actuation. In Section IV, we investigate the anchoring capabilities of the actuator segments. In Section V, we explore the locomotion of the multi-segmented robots on the surface of and inside GM. In addition, in Section VI, we demonstrate the self-sensing capabilities of the actuator segments. Finally, in Section VII, we analyze the power consumption of our system to investigate the feasibility of untethered operation of our robot design.

II. Design and Fabrication

We fabricated our robots with a modular design, consisting of individual actuator segments (Figure 1). We used circular, expanding HASEL actuators for our system [15]. When we applied an electrical potential between each set of electrodes, the induced electrostatic force attracted the electrodes of each HASEL together. This pushed the dielectric liquid to the remaining areas of the flexible pouches, inducing hydraulic pressure that resulted in positive strain in the direction normal to the surface of the electrodes (Figure 1A). With this geometry, actuation strain can be $> 100\%$. However, individual layers of expanding actuators are thin—typically 1 mm or less. Thus, we stacked multiple layers of HASELs to increase the total displacement.

Each of the actuator segments consisted of 20 of these stacked HASELs and were capped at either end with polymer end caps, which also housed electrical connections for the electrodes (Figure 1B). The end caps were 3D-printed with resin-based stereolithography (Formlabs Black Resin V5) to ensure water-tight assembly to allow underwater operation of the actuators. Four elastic bands (2.5 oz light orthodontic bands) tied the end caps together to provide restoring force when the actuators were at the resting state. In addition, flexible membrane made from thermoplastic urethane (TPU) was attached to protect and electrically insulate the HASELs from the surrounding environment.

We assembled each multi-segmented robot with five to seven of these actuator segments and attached a 3D-printed conical tip on the front end (Figure 1C). The diameter of the anterior cone and the polymer end caps of each segment was $\varnothing$61 mm, while the HASEL actuators inside had diameter of $\varnothing$50 mm. The length of the front cone was equal to its diameter (61 mm), while the length of each segment was 31.5 mm when the actuators were at rest.

Each segment of the robot could be individually actuated using a multi-channel high-voltage power supply (HVPS, PS2-08-A model, Artimus Robotics) (Figure 1C). This allowed us to freely tune the input voltage signals and the gait of the multi-segmented robots. We used either peristaltic or uniform gaits to operate the assembled robot. During the peristaltic gait, the anterior segments expanded first in each cycle, then the following segments sequentially expanded as the previous segments contracted, creating peristaltic waves that propagated posteriorly. For uniform gaits, we actuated each segment simultaneously with in-phase sinusoidal voltage inputs.

III. Intruder Drag Tests in Dry and Submerged Granular Media

To characterize the drag reduction effects of the high-frequency HASEL actuation in granular media (GM), we first fabricated intruders, each with a single actuator segment. We then dragged the intruders through dry and submerged GM with various actuation modes and recorded the resultant drag forces.

A. Drag test method and design of intruders

For the intruder drag tests, we used an industrial robot (UR16e, Universal Robots) with a six-axis force/torque sensor (ATI Industrial Automation) on the end-effector, and fixed the intruders to the force/torque sensor (Figure 2A). The robot arm dragged the intruders horizontally through the GM at the depth of 40 mm at a constant speed of 1 mm/s. We recorded and analyzed the resultant drag force in the direction opposite of the movement of the intruders.

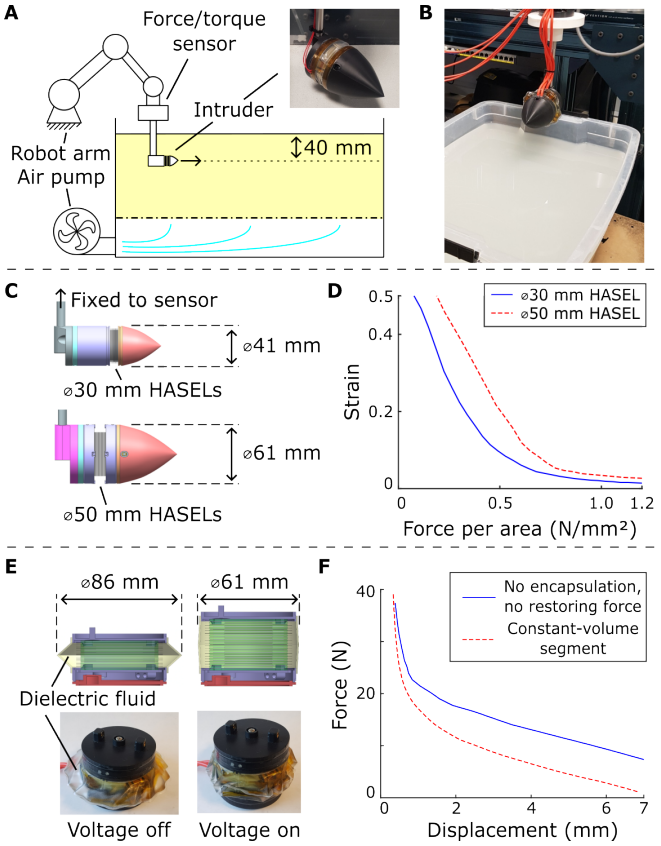

Fig. 2. Drag test method and design of intruders. A) Test setup for the tests in dry GM. We fixed the intruders to a force/torque sensor, which was connected to a robot arm. We recorded the force measurements from the sensor as the arm dragged the intruder horizontally through the GM. We used the air pump to reset the granular substrate before each test. B) Setup for the tests in submerged GM. C) Dimensions and specifications of the two versions of intruders used for the tests in dry GM. D) Comparison of the force per area vs. strain response of the two types of HASEL actuators used. E) We used constant-volume segments for the tests in submerged GM. We filled the internal volume of these segments with dielectric fluid to allow underwater operation. F) Comparison of the displacement vs. force output performances of the constant-volume segments and the segments without encapsulation or the internal elastic bands, actuated at 6 kV.

For the granular substrate, we used glass beads of diameter 300 µm to mimic the particle size of medium sand (200 µm to 630 µm according to ISO14688-1:2017). For intruder tests in dry GM, we used a test bed made with acrylic, with dimensions 420 mm × 420 mm wide and maximum GM depth of 350 mm. The test bed was integrated with an air pump that we used to fluidize the entire substrate to a uniformly packed state before each experiment for more consistent results (Figure 2A). For the tests in submerged GM, we used a test bed of dimensions 370 mm x 270 mm wide, with maximum GM depth of 200 mm and water level 50 mm above the surface of GM (Figure 2B). This setup for submerged GM, unlike the one for dry GM, did not have an integrated mechanism to fluidize the substrate, and we manually raked the GM to reset the packing ratio before each test.

We made each intruder with a single actuator segment and attached a 3D-printed rigid cone to the front (Figure 2). We also fixed each intruder to a stainless steel rod in the rear, which was then connected to the force/torque sensor. We used the rod of length 152.4 mm to allow sufficient clearance between the sensor and the surface of the GM.

For the tests in dry GM, we used two versions of the intruders, a smaller one made with HASELs of diameter ⌀30 mm and a larger one made with those of diameter ⌀50 mm (Figure 2C). This resulted in the overall diameter of the intruders of ⌀41 mm and ⌀61 mm, respectively. We found that the larger HASEL actuators exhibited larger force per area for the same strain and input voltage (Figure 2D). In this study, we did not consider HASELs of diameters greater than ⌀50 mm due to the challenges associated with even larger HASELs; the internal dielectric fluid could sag to different parts of the flexible pouch, leading to poor performance characteristics, and the actuators would require more energy to operate due to higher capacitance.

For the drag tests in *submerged* GM, we fabricated actuator segments with modified design to allow underwater operation. We filled the internal volume of the segment with dielectric fluid to resist the hydrostatic pressure underwater and for enhanced electrical insulation of the electrodes (Figure 2E). Due to the incompressible nature of this fluid, these segments maintained their volume in different states of actuation, and thus we named them constant-volume segments. This modification also caused the cross-sectional area to vary with actuation. We only used the larger HASELs of diameter ⌀50 mm for these segments, and the overall diameter varied between ⌀86 mm when the actuators were at rest and ⌀61 mm when they were fully actuated. We found out that for the same input voltage of 6 kV, these segments exhibited decreased force output compared to those without encapsulation or internal elastic bands, particularly at higher displacement regions (Figure 2F).

During the tests, we actuated the intruders with sinusoidal voltage inputs oscillating between 0 and 6 kV at frequencies: 1, 10, 20 Hz for the smaller intruder in dry GM and 10 Hz for the larger intruder in dry GM, as well as the intruders in submerged GM. We also repeated the tests with unactuated intruders to compare the results.

B. Drag reduction effects of high-frequency HASEL actuation in dry GM

We first performed the drag tests in dry GM using the smaller intruders (made with ⌀30 mm diameter HASELs). In these tests, the resultant drag steadily increased for the initial 60 to 80 seconds, after which it showed little variation (Figure 3A). We analyzed the steady-state drag forces over 100 to 200 seconds for each actuation mode. The average drag measured for the unactuated intruder was 8.29±0.20 N. Vibrating the intruder at 10 Hz decreased the drag to 6.43±0.22 N, which was lower by 1.86 N, or 22.4%. Increasing the actuation frequency above 10 Hz did not result in significant further reduction of drag forces; the intruder vibrating at 20 Hz exhibited drag of 6.34±0.26 N. We think that this might be due to the vibration amplitude of the burrowed intruder falling off at these frequency ranges. When

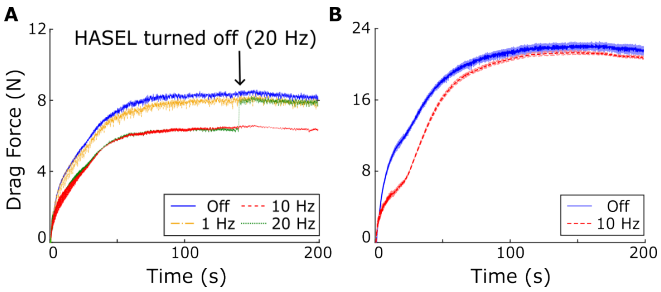

Fig. 3. Results from the intruder drag tests in dry GM. A) Representative drag force measurements with the smaller intruders (with ⌀30 mm diameter HASELs). We tested the intruders in four different actuation modes: unactuated and vibrating at 1, 10, and 20 Hz. When the HASELs were turned off during the 20 Hz test, the drag force immediately increased. B) Drag force measurements with the larger intruders (with ⌀50 mm diameter HASELs), unactuated and vibrating at 10 Hz.

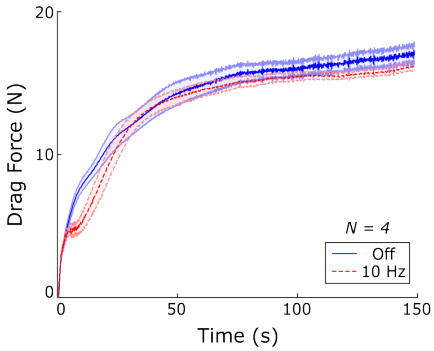

Fig. 4. Results from the intruder drag tests in submerged GM over $N = 4$ trials. The intruders were dragged through the substrate either with the HASELs turned off (blue) or vibrating at 10 Hz (red).

we turned off the actuators in the middle of a 20 Hz test, the drag forces immediately increased to 7.93±0.19 N for the remainder of the test. Low frequency actuation of 1 Hz resulted in drag force of 7.94±0.18 N, showing relatively little drag reduction of 0.35 N, or 4.2% from the unactuated case.

We then tested the drag forces in dry GM using the larger intruders (made with HASELs of diameter ⌀50 mm). In these tests, the resultant drag initially increased for about 100 seconds, after which it was relatively stable (Figure 3B). Over the region of 100 to 200 seconds, the average drag force of the unactuated intruder was 20.60±0.44 N. Vibrating the HASELs at 10 Hz reduced the drag to 18.48±0.26 N, which was lower by 2.12 N or 10.3%.

The intruder test results in dry GM showed that the high-frequency actuation of the HASEL segments significantly reduced the drag forces. The smaller intruders showed higher proportional drag reduction (22.4% with 10 Hz actuation) compared to the larger intruders (10.3% with 10 Hz actuation). This is because the actuation of larger intruders resulted in average drag reduction (2.12 N) only slightly larger in magnitude compared to that of smaller intruders (1.86 N), while the magnitude of total drag force increased in similar proportion with the increased surface area of the larger intruders (increase of overall diameter from ⌀41 mm to ⌀61 mm, corresponding to ×2.21 surface area).

This comparison presented a trade-off between the HASELs of ⌀30 mm and ⌀50 mm for the use on multi-segmented robot. While the intruders with smaller HASEL actuators exhibited proportionally higher drag reduction with high-frequency actuation (Figure 3), the larger HASELs achieved higher strain for the same normalized force output (Figure 2D). After considering each point, we implemented the larger ⌀50 mm HASELs for the robot; the results of the drag tests demonstrated their potential for drag reduction, and the stroke of actuation was an important consideration for the burrowing robot.

C. Drag reduction effects of high-frequency HASEL actuation in submerged GM

The intruder tests in submerged GM showed the drag forces increasing for the duration of the entire test for both actuation modes of unactuated and vibrating at 10 Hz (Figure 4). We analyzed the measurements over 100 to 150 seconds, where the rate of change of drag was lower. Over this region, the mean drag increased from 16.03 N to 16.94 N when the intruder was unactuated and from 15.47 N to 16.19 N when the intruder was vibrating at 10 Hz. The average difference of drag force between each actuation mode over this region was 0.83±0.18 N.

While the magnitude of drag in submerged GM (15.47 to 16.94 N, over 100 to 150 seconds) was lower than that in dry GM (18.48 to 20.60 N, over 100 to 200 seconds), the magnitude of drag reduction due to high-frequency HASEL actuation was also significantly lower in submerged GM (0.83±0.18 N) than in dry GM (2.12 N). We think that this might be due to the damping effects from water surrounding the GM particles.

IV. Expansion-anchoring effects of constant-volume actuator segments

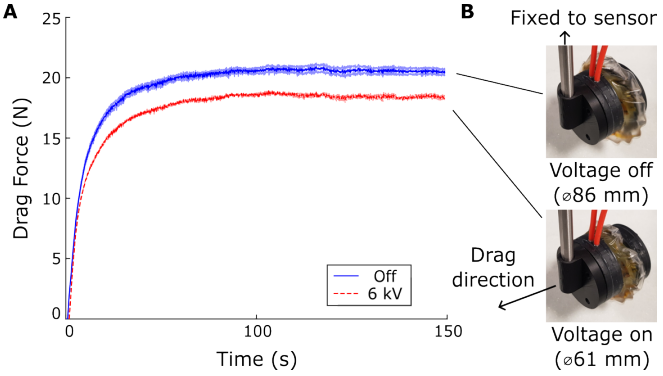

Fig. 5. Expansion-anchoring effects of the constant-volume actuator segments. A) Drag force measurements of the segments, unactuated vs. constant voltage (6 kV), in dry GM. B) Images of the segments, showing both increase in length and decrease in diameter when the voltage is applied.

A large degree of asymmetry in drag forces plays a key role in enabling burrowing locomotion in GM. One way to achieve this asymmetry is through anchoring, where certain parts of the robot amplify drag to direct the actuation stroke toward the desired direction of travel. For the peristaltic gait of the multi-segmented robot described in Section II, it is important for the posterior segments to anchor in GM while the anterior segments undergo actuation. Since the constant-volume segments expand radially when the actuators are at rest, they show potential for anchoring effect for our robot design.

To evaluate this capability, we performed drag tests using the constant-volume segment in dry GM. Similar to the intruder drag tests in described in Section III-A, we fixed the segment to the force/torque sensor, dragged the segment through the GM, and measured the resultant forces (Figure 5B). We tested the segment in two different states, unactuated and fully actuated with constant input voltage of 6 kV.

Similar to the results of the intruder tests in dry GM, the resultant drag for both of these cases increased for the initial 70 to 80 seconds, after which it showed little variation (Figure 5A). We analyzed the steady-state drag forces over 100 to 200 seconds. When unactuated, the segment experienced drag forces of 20.60±0.41 N in this region. When fully actuated, the average drag decreased to 18.48±0.21 N, showing average difference of 2.14 N.

This substantial difference in drag demonstrated the capability of the constant-volume segments to achieve anchoring through radial expansion. For the multi-segmented robot, this anchoring effect would be multiplied by the number of the segments that are unactuated during the peristaltic gait. We think that this effect could potentially be enhanced by changing the design of the encapsulating TPU membrane or by adding asymmetrically shaped bristle-like structures to the membrane.

V. Locomotion tests of Multi-segmented Robots

We tested the locomotion properties of the prototype multi-segmented robots on the surface of, and burrowing into, both dry and submerged GM. During these tests, we had the first segment continuously vibrate at a frequency of 10 Hz, similar to how the intruders were actuated during the drag tests. We operated the rest of the segments using either peristaltic or uniform gait as described in Section II.

A. Locomotion on the surface of dry and submerged GM

For the locomotion tests on the surface of dry GM, we used the robot with six segments (only encapsulated with membrane and not filled with dielectric fluid). We actuated the robot on the surface of dry GM using peristaltic gait of frequency 3 Hz and phase between segments 60°. The robot moved forward 53 mm over 55 seconds, averaging at 0.96 mm/s, or 0.32 mm per each peristaltic gait cycle (Figure 6A).

For the locomotion test on the surface of *submerged* GM, we used the robot with seven constant-volume segments. We maintained the water level 30 mm above the surface of GM

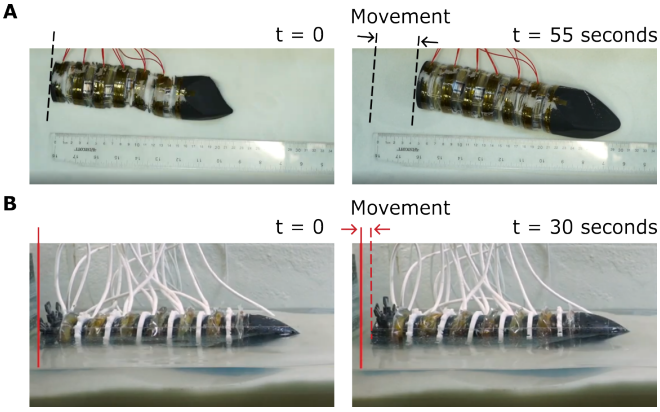

Fig. 6. Locomotion of the multi-segmented robots on the surface of dry and submerged GM. A) The robot with six segments traveled 53 mm on the surface of dry GM over 55 seconds. B) The robot with seven constant-volume segments traveled 13.6 mm on the surface of submerged GM over 30 seconds.

to limit the effects of buoyancy, since the constant-volume segments, filled with dielectric oil, had slightly less density compared to water. We also added 3D-printed radial fins of length 7 mm between the segments and fins of length 19.5 mm at the rear end of the robot to enhance the frictional forces between the robot and the GM. With peristaltic gait of frequency 0.5 Hz and phase between segments 180°, the robot moved forward 13.6 mm over 30 seconds, averaging at 0.45 mm/s, or 0.23 mm per each peristaltic gait cycle (Figure 6B).

These results showed the ability of the multi-segmented robots to achieve forward locomotion on the surface of GM, albeit slowly. Although each segment was capable of achieving large displacement—7 mm or higher in no load condition at input voltage of 6 kV (Figure 2F)—actuation on granular surface resulted in substantial slip in each cycle, limiting the overall speed of the robot.

B. Burrowing locomotion in dry and submerged GM

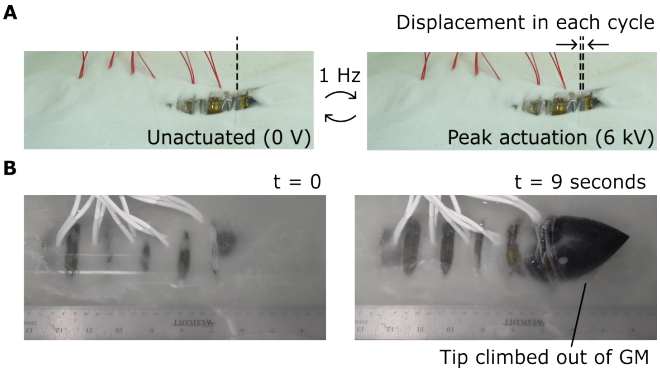

Fig. 7. Locomotion of the multi-segmented robots inside GM. A) When actuated with uniform gait inside dry GM, the robot expanded and contracted longitudinally in both directions, but did not achieve measurable forward locomotion over time. B) Starting the robot from a fully buried position inside submerged GM made one end rapidly climb out of GM. Afterwards, the robot wiggled in place and did not exhibit net locomotion.

For the burrowing tests in dry GM, we used the robot

with six segments (not filled with dielectric fluid) and actuated it with both peristaltic and uniform gaits. When we used peristaltic gait, we observed limited displacement of each segment (∼1 mm). Regardless of how we tuned the frequency of the gait, the segments wiggled in place and the robot did not move forward over time. We then repeated the test with uniform gait of frequency 1 Hz to amplify the displacement of the robot. During these tests, the robot expanded and contracted longitudinally in both directions. We observed slightly larger peak-to-peak displacement (∼3 mm) of the first and last segments in each cycle (Figure 7A). However, as the robot contracted back to the same position after each expansion, it did not achieve measurable forward locomotion over time.

We attributed the limited displacement of the robot in dry GM with peristaltic gait to the high level of drag forces of the surrounding substrate. The results of the intruder drag tests showed that even with the high-frequency actuation of the first segment, the robot would still need to overcome up to ∼20 N of drag force to burrow forward in dry GM (Figure 3B). Under this load, the displacement of each actuator segment was limited to 2 mm or less with the operation voltage of 6 kV (Figure 2F). While the use of uniform gait increased the peak-to-peak displacement of the first and last segments in each cycle, it also caused the entire robot to expand and contract at the same time. Because of this, the robot needed higher degree of asymmetry in drag forces if it was to achieve net forward locomotion. We think that to address these issues, future work could explore alternative configurations of the HASEL actuators to gain mechanical advantage for enhanced force or stroke output, or different actuation modes for the segments, combining low- and high-frequency signal inputs.

We also tested the burrowing locomotion of the robot in *submerged* GM, where our previous intruder drag tests had shown to exhibit less drag force compared to the dry substrate (Figure 4). We used the robot with five constant-volume segments and used peristaltic gait of frequency 1 Hz. When we started the robot, the front end of the robot climbed rapidly out of GM (Figure 7B). Afterwards, the robot wiggled in place and did not exhibit net locomotion. We observed similar behaviors after tuning the density of different parts of the robot. When we repeated the tests after adding weights to the front tip, the rearmost segment climbed out of GM, after which the robot wiggled in place. When we added weights to both the first and the last segments, the middle section of the robot climbed out of GM.

We attributed this phenomenon to the high flexibility of the multi-segmented robot design. Each segment was only held together by the internal elastic bands and the encapsulating membrane, and therefore was free to bend in place. Because of this, without any structure along the longitudinal axis to provide rigidity, a part of the robot prematurely climbed out of GM due to the effects of buoyancy and the pressure gradient within the surrounding substrate, causing the entire system to get stuck. We think that the future iterations of this robot could potentially address this issue by adding a stiffness tuning structure along the longitudinal axis of the body.

VI. Demonstration of Self-Sensing Capability

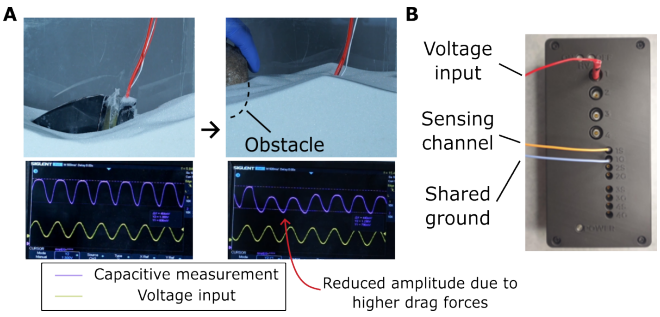

Fig. 8. Demonstration of self-sensing capability of the actuator segments. A) The capacitive measurements exhibited change in amplitude in response to the increased drag forces due to the addition of the obstacle. B) The modified HVPS used for both actuation and sensing of the intruder. Only one additional wire connection was required to achieve self-sensing.

We demonstrated the use of self-sensing capability of our HASEL segments to detect obstacles in GM using an intruder and a modified HVPS with self-sensing circuitry (PS2-04-S model, Artimus Robotics) (Figure 8). When we operated the intruder with a sinusoidal voltage input on the surface of the GM, the capacitative measurement showed the corresponding sinusoidal actuation of the segment (Figure 8A, left). When we increased the drag forces by covering the intruder with GM and pushing an obstacle in front of the the tip, the measurement reading reflected this with sinusoidal output of reduced amplitude, showing the decrease in strain in response to the change in surroundings (Figure 8A, right).

We achieved this self-sensing capability with minimal modification of the HVPS and one additional wire connection (Figure 8B); to operate n segments each with self-sensing capability, the system would need $2n + 1$ connections, n for voltage input, n for capacitive sensing, and 1 for shared ground. This scales better with the increase in number of segments compared to incorporating separate sensor units for each segment.

VII. Analysis of Power Consumption

The rate of power consumption is an important consideration for untethered robotic platforms, which have to carry the power supply onboard. We analyzed the power consumption of our system to investigate the feasibility of the untethered design of our approach and to determine the estimated operational endurance.

We estimated the average power P as the energy required to charge an equivalent capacitor divided by the charging time t_c:

$$P = \frac{1}{2} C V^2 \cdot \frac{1}{t_c}$$

Each segment consisted of 20 HASEL actuators of diameter of ⌀50 mm, which had circular electrodes of diameter ⌀30 mm and therefore effective electrode area A = 7.07 mm^2.

Using film thickness of t = 15 µm and relative material permittivity ϵ_r = 3.3, we calculated the maximum capacitance of each actuator segment:

$$C = \frac{20\epsilon_0\epsilon_r A}{2t} = 14 \text{ nF}$$

During the operation of the multi-segmented robot with peristaltic gait of frequency 0.5 Hz and phase between segment 180°, one of the posterior segments was being charged at a given time over $t_c = 0.4$ seconds. The first segment, continuously vibrating at 10 Hz, was being charged over $t_c = 0.05$ seconds for half of the operation time. Thus, with input voltage V = 6 kV, we estimated the average power consumption of the robot to be:

$$P_{average} = P_{peristaltic} + \frac{1}{2}P_{first} = 3.15 \text{ W}$$

and the peak power consumption to be:

$$P_{peak} = P_{peristaltic} + P_{first} = 5.67 \text{ W}$$

For the real system, the power consumption is not limited to the actuators but also includes the components of the HVPS, such as high-voltage amplifiers, switches, microcontrollers, and regulators. To measure the actual power consumption of our entire system, we used a desktop power supply that powered the HVPS, and by extension, the multi-segmented robot as well. While the robot was idling, the measured power consumption of the system was 2.2 W. During the operation of the robot, the power consumption continuously fluctuated as the actuators were being charged and discharged, peaking at 9.2 W. With this measured peak value, we deduced that with a commercial USB-C 5 V, 20000 mAh power bank, our system would have operational endurance of at least 10.7 hours.

VIII. Conclusion and Future Work

In this paper, we explored the use of HASEL actuators for soft robots capable of burrowing in dry and submerged GM. We first presented a prototype design of HASEL-based actuator segments and multi-segmented robots. We performed drag tests to analyze the drag reduction effects of high-frequency HASEL actuation in GM and to investigate the expansion-anchoring effects of the constant-volume segments. We then studied the locomotion of the multi-segmented robots both on the surface of and inside GM. We also demonstrated the self-sensing capability of the actuator segments to detect obstacles within GM. Finally, we analyzed the power consumption of our system and estimated its operational endurance.

During the study we have found the following limitations of our design that could be addressed in future work. We made each actuator segment by stacking multiple HASEL layers to increase effective stroke, with the electrodes of each HASEL in contact with those of the adjacent ones (Figure 1B). Because of this configuration, if one of the HASELs broke down in a way that introduced an internal short between the electrodes, this would lead to the failure of the entire segment. Furthermore, because the electrodes were exposed within the internal structure of the segment, proper encapsulation of the segment was critical, especially for the tests conducted underwater. Alternative designs to better protect and insulate the HASELs could improve the reliability of the system and simplify fabrication.

Another potential avenue for future improvement is the development of HASEL actuators with higher force and strain output. There is extensive ongoing research encompassing material science and mechanics of thin film materials to enhance the performance of HASELs. For example, the use of higher permittivity dielectric materials for the flexible pouches could increase the maximum force output of these actuators. Producing such materials with high breakdown strength and consistent performance is an ongoing challenge, and thus they were not used in this study. However, such improvements in the future, combined with optimized design of the robot, may make it possible to achieve forward burrowing locomotion within GM using HASELs.

References

[1] Gravish, N., Umbanhowar, P. B., Goldman, D. I. "Force and Flow Transition in Plowed Granular Media", *Phys. Rev. Lett.*, vol. 105, issue 12, pp 128301, 2010.

[2] Le, C.L., Yirmibesoglu, O.D., Even, S., Buckner, T., Ozkan-Aydin, Y., Kramer-Bottiglio, R. "Grand challenges for burrowing soft robots",*Frontiers in Robotics and AI*, vol. 12, 2025.

[3] Trueman, E.R., Brand, A.R., Davis, P. "The Dynamics of Burrowing of Some Common Littoral Bivalves", *Journal of Experimental Biology*, vol. 44, issue 3, pp. 469-492, 1966

[4] Macdonald, I. "Burial mechanics of the Pacific sandfish: The role of the ventilatory pump and physical constraints on the behavior", *Master's thesis*, Northern Arizona University, 2015

[5] Winter, A.G., Deits, R.L.H., Dorsch, D.S. "Critical Timescales for Burrowing in Undersea Substrates via Localized Fluidization, Demonstrated by RoboClam: A Robot Inspired by Atlantic Razor Clams", *Proceedings of the ASME 2013 International Design Engineering Technical Conferences and Computers and Information in Engineering Conference. Volume 6A: 37th Mechanisms and Robotics Conference*, Portland, Oregon, USA. 2013

[6] Montana, J., Finn, J.K., Norman, M.D. "Liquid sand burrowing and mucus utilisation as novel adaptations to a structurally-simple environment in Octopus kaurna Stranks", *Behavior*, vol. 152, pp. 1871-1881, 2015

[7] Naclerio, N.D., Karsai, A., Murray-Cooper, M., Ozkan-Aydin, Y., Aydin, E., Goldman, D. I., Hawkes, E. W. "Controlling subterranean forces enables a fast, steerable, burrowing soft robot", *Science Robotics*, vol. 6, issue 55, 2021

[8] Nayak, A., Seo, H., Gravish, N., Tolley, M.T. "Burrowing and unburrowing in submerged granular media through fluidization and shape-change", *Frontiers in Robotics and AI*, vol. 12, 2025

[9] Helal, K., Biben, T., Hansen, J.P. "Local fluctuations in a fluidized granular medium", *Physica A: Statistical Mechanics and its Applications*, vol. 240, issues 1-2, pp. 361-373, 1997

[10] Hashemnia, K., Pourandi, S. "Study the effect of vibration frequency and amplitude on the quality of fluidization of a vibrated granular flow using discrete element method", *Powder Technology*, vol. 327, pp. 335-345, 2018

[11] Savage, S.B., "Streaming motions in a bed of vibrationally fluidized dry granular material", *Journal of Fluid Mechanics*, vol. 194, pp. 457-478, 1988

[12] Liu, B., Wang, T., Kerimoglu, D., Kojouharov, V., Hammond, F.L., Goldman, D.I. "Robust self-propulsion in sand using simply controlled vibrating cubes", *Frontiers in Robotics and AI*, vol. 11, 2024

[13] Texier, B.D., Ibarra, A., Melo, F. "Low-resistive vibratory penetration in granular media", *PLOS One*, vol. 12, issue 4, 2017

[14] Li, D., Tolley, M.T., Gravish, N. "Autonomous Burrowing and Retrieval of Soft Robotic Anchors in Granular Media", *2025 IEEE 8th International Conference on Soft Robotics (RoboSoft)*, Lausanne, Switzerland, pp. 1-7, 2025

[15] Acome, E., Mitchell, S.K., Morrissey, T.G., Emmett, M.B., Benjamin, C., King, M., Radakovitz, M,, Keplinger, C. “Hydraulically amplified self-healing electrostatic actuators with muscle-like performance”, *Science*, vol. 359, issue 6371, pp. 61-65, 2018.

[16] Rothemund, P., Kellaris, N., Mitchell, S.K., Acome, E., Keplinger C. “HASEL Artificial Muscles for a New Generation of Lifelike Robots-Recent Progress and Future Opportunities”. *Advanced Materials*, vol. 33, 2021

[17] Kellaris, N., Venkata, V.G., Smith, G.M., Mitchell, S.K., Keplinger, C. “Peano-HASEL actuators: Muscle-mimetic, electrohydraulic transducers that linearly contract on activation”, *Science Robotics*, vol. 3, issue 14, 2018

[18] Mitchell, S.K. Wang, X., Acome, E.,, Martin, T., Ly, K., Kellaris, N., Venkata, V.G., Keplinger, C. “An Easy-to-Implement Toolkit to Create Versatile and High-Performance HASEL Actuators for Untethered Soft Robots”, *Advanced Science*, vol. 6, 2019

[19] Vogt, M.R., Eberlein, M., Christoph, C.C., Baumann, F., Bourquin, F., Wende, W., Schaub, F., Kazemipour, A., Katzschmann, R.K. “High-Frequency Capacitive Sensing for Electrohydraulic Soft Actuators”, *2024 IEEE/RSJ International Conference on Intelligent Robots and Systems (IROS)*, Abu Dhabi, UAE, 2024

[20] Ly, K., Kellaris, N., McMorris, D., Johnson, B.K., Acome, E., Sundaram, V., Naris, M., Humbert, J.S., Rentschler, M.E., Keplinger, C., Correll, N. “Miniaturized Circuitry for Capacitive Self-Sensing and Closed-Loop Control of Soft Electrostatic Transducers”, *Soft Robotics*, vol. 8, no. 6, 2021

[21] Kazemipour, A., Hinchet, R., Katzschmann, R.K. “Stretchable Electrohydraulic Artificial Muscle for Full Motion Ranges in Musculoskeletal Antagonistic Joints”, *2025 IEEE International Conference on Robotics and Automation (ICRA)*, Atlanta, USA, 2025

[22] Yoder, Z., Kellaris, N., Chase-Markopoulou C., Ricken, D., Mitchell, S.K., Emmett, M.B., Weir, R.F.ff., Segil, J., Keplinger, C. “Design of a High-Speed Prosthetic Finger Driven by Peano-HASEL Actuators”, *Frontiers in Robotics and AI*, vol. 7, 2020

[23] Christoph, C.C., Kazemipour, A., Vogt, M.R., Zhang, Yu., Katzschmann, R.K. “Self-Sensing Feedback Control of an Electrohydraulic Robotic Shoulder”, *2024 IEEE International Conference on Robotics and Automation (ICRA)*, Yokohama, Japan, 2024.

[24] Buchner, T.J.K., Fukushima, T., Kazemipour, A., Gravert, S., Prairie, M., Romanescu, P., Arm, P., Zhang, Y., Wang, X., Zhang, S.L., Walter, J., Keplinger, C., Katzschmann, R.K. “Electrohydraulic musculoskeletal robotic leg for agile, adaptive, yet energy-efficient locomotion”, *Nature Communications*, vol. 15, no. 7634, 2024

[25] Hess, I., Musgrave, P. “A continuum soft robotic trout with embedded HASEL actuators: design, fabrication, and swimming kinematics”, *Smart Materials and Structures*, vol. 33, 2024

[26] Cooney, R.M., Hesam, M., Anderson, I.A. “HASEL actuators for underwater robots”, *Electroactive Polymer Actuators, Sensors, and Devices (EAPAD) 2025*, Vancouver, B.C., Canada, 2025

[27] Yoder, Z., Rumley, E.H., Schmidt, I., Rothemund, P., Kelplinger, C. “Hexagonal electrohydraulic modules for rapidly reconfigurable high-speed robots”, *Science Robotics*, vol. 9, 2024

[28] Wu, Y., Sun, Z., Xiang, Y., Zhao, J. “AWorm-like Soft Robot Based on Adhesion-Controlled Electrohydraulic Actuators”, *Biomimetics*, vol. 9, no. 12, pp. 776, 2024